Computational Investigation of the Near-Field Plasma Plume in Ion-Ion Propulsion

K. Sankaran*, T. Widmer†, and T. Dale‡
Whitworth University, Spokane, WA 99251

K. A. Polzin§
NASA Marshall Space Flight Center, Huntsville, AL 35812

A two-fluid numerical model of plasma flows was developed to investigate the plume of an ion-ion propulsion system. The densities of positive and negative ions, and the associated values of net charge, electric field, and electric potential were calculated as a function of time throughout the domain. The computational domain was chosen to be large enough (25 thruster diameters downstream of the exit plane) to allow for examining the neutralization of the plume. The resulting plasma electric potential and charge neutrality at the downstream end of the domain are shown and they indicate that it is possible to alternatively accelerate oppositely charged ions without the need for an electron-emitting neutralizer and without facing any electric potential hills that could cause stagnation. However, compared to existing literature on ion-ion plasma thrusters, the results from this simulation predict a longer length-scale for voltage decay.

Nomenclature

$(\ldots)_{p,n}$	=	positive and negative ions
$\mathcal{D}$	=	mass diffusivity (m^2/s)
e	=	elementary charge (C)
$\mathcal{E}$	=	thermal energy + kinetic energy, per unit volume (J/m^3)
$\mathbf{f}_{\text{ext}}$	=	external force, per unit volume (N/m^3)
$\bar{\bar{I}}$	=	identity matrix
$m_{p,n}$	=	mass of a particle (kg)
$n_{p,n}$	=	number density of particles ($\#/m^3$)
$p_{p,n}$	=	thermodynamic pressure (Pa)
$\dot{q}$	=	power transfer, per unit volume ($J/s/m^3$)
$\mathbf{u}$	=	velocity (m/s)
V	=	electric potential (V)
$\epsilon_\circ$	=	electrical permittivity ($C^2/N\ m^2$)
γ	=	ratio of specific heats (#)
ν_{coll}	=	collision frequency (#/s)

I. Introduction

Electric propulsion systems that electrostatically accelerate the propellant, such as conventional ion thrusters, expel a beam of positive ions and thus require neutralization of the exhaust. This is typically accomplished by the emission of electrons from a cathode that is placed slightly downstream of the accelerating grids. An electrostatic acceleration mechanism that does not require a neutralizer would be beneficial in reducing the complexity of the thruster system and eliminating a potential point of failure. To that end, a thruster in which packets of positive and

*Professor; Senior Member of AIAA.
†Student.
‡Student.
§Research Engineer; Associate Fellow of AIAA.

negative ions are successively expelled by varying the electric potential of the accelerating grid was proposed by Aanesland, *et al.*[1]. Further refinements to this accelerator concept have led to the development of devices such as the "Plasma propulsion with electronegative gases" (PEGASES)[2] that have been theoretically and experimentally investigated[3]. The possibility of neutralizing the plasma plume[4] without the need for an external neutralizer leads us to investigate the efficacy of the neutralization process. Oudini, *et al.*[5] investigated this mechanism using a two-dimensional particle-in-cell (2D-PIC) simulation and showed that there is a well-defined range of bias frequencies to ensure downstream acceleration of the plasma, and also that effective neutralization of the plume occurs approximately 10 cm downstream of a 2 cm × 2 cm square acceleration grid. In this paper, we seek to revisit the results of Oudini, *et al.*[5] using a two-fluid simulation to clarify three questions:

1) How does the electrical potential decay downstream of the thruster?
2) How do the results change when the model is changed from 2D-PIC (with weighted particles) to a 2D-axisymmetric two-fluid simulation?
3) What are the effects of classical transport on the behavior of the plume?

In this paper we describe our efforts to examine these three questions and presents the results of our investigations to date. Section II describes the characteristics of the specific thruster that was simulated. Section III describes the mathematical and numerical model of the plasma flow in the plume. Section IV presents the results of our two-fluid simulations.

II. Thruster Characteristics

To allow for a valid comparison with the results of Ref. [5], the same thruster specifications were chosen in this work. A notable difference between this work and that of Ref. [5] is that, since a cylindrical cross-section is more common than a square cross-section in propulsive applications, we chose to model a thruster with a cylindrical geometry and an exit radius of $r_{\text{thruster}} = 1$ cm (instead of a 2 cm × 2 cm square exit). Furthermore, to reduce the sharp gradients in voltage (and, thus, strong electric fields near the thruster exit), our model included an insulated ring of $r_{\text{insul}} = 2$ cm around the thruster exit.

As in Ref. [5], the propellant in this simulation was iodine, with alternating fluxes of I^+ and I^- ions injected into the domain. The bias voltage of the grid was set to $V_{\text{accel}} = \pm 500$ V. Though Oudini, *et al.*[5] considered a range of bias frequencies from 0.5-2.0 MHz, we only simulated the grid bias frequency of $f_{\text{bias}} = 1.25$ MHz ($T_{\text{bias}} = 0.8$ μs) in this work.

The plasma upstream of the grid was taken to be accelerated electrostatically (by $V_{\text{accel}} = 500$ V) and then injected into the computational domain. The plasma characteristics immediately downstream of the grid (upstream boundary of the simulation) were also chosen to match the values used in Ref. [5]. The temperature of both the positive and negative ions at the inlet were set to $T_{p,n} = 0.1$ eV. The inlet velocity was purely axial at $\mathbf{u}_{p,n} = \sqrt{2eV_{\text{accel}}/m_{p,n}}\,\hat{\mathbf{z}}$. Using the values given in Ref. [5] for density and ion thermal velocity upstream of the grid, and the inlet propellant velocity, the density at the inlet was calculated using mass conservation to be $n_{p,n} = 10^{15}\text{m}^{-3}$. The simulation parameters are summarized in Table 1.

Table 1 Simulation Parameters

Ion-ion density (inlet)	$10^{15}/\text{m}^3$
Ion temperature (inlet)	0.1 eV
Ion mass	126.9 amu
Acceleration voltage (upstream)	500 V
Ion axial speed (inlet)	27474 m/s
Thruster inlet radius	1 cm
Insulator ring outer radius	2 cm
Acceleration grid bias frequency (Square wave)	1.25 MHz

III. Computational Model

The ion-ion propulsion system described in Aanesland, *et al.* [1] uses magnetic filtering to ensure that the free electron density is negligible in the exhaust. Consequently, we follow the approach of Oudini, *et al.*[5] and treat the plasma as being comprised only of positive and negative iodine ions. Under these assumptions, the governing equations for conservation of mass, momentum, and energy in an infinitesimal volume are,

$$\frac{\partial}{\partial t}\begin{bmatrix} n \\ n\mathbf{u} \\ \mathcal{E} \end{bmatrix}_{p,n} + \nabla\cdot\begin{bmatrix} n\mathbf{u} \\ n\mathbf{u}\mathbf{u} + \frac{p}{m}\bar{\bar{I}} \\ (\mathcal{E}+p)\,\mathbf{u} \end{bmatrix}_{p,n} = \begin{bmatrix} \mathcal{D}\nabla^2 n \\ \frac{\mathbf{f}_{\text{ext}}}{m} \\ \dot{q} \end{bmatrix}_{p,n}. \tag{1}$$

Here, the external force per unit volume due to electric fields and collisions is $\mathbf{f}_{\text{ext}} = \pm n_{p,n}\left(e\mathbf{E} - m_{p,n}\nu_{\text{coll}}\mathbf{u}\right)$. Oudini, *et al.*[5] assumed that collisions were negligible. If so, the external force per unit volume reduces to $\mathbf{f}_{\text{ext}} \simeq \pm n_{p,n}e\mathbf{E}$. For each species, the energy (thermal + kinetic) per unit volume is,

$$\mathcal{E} = \mathcal{E}_{\text{therm}} + \mathcal{E}_{\text{kin}} = \frac{p}{\gamma-1} + \frac{1}{2}nmu^2. \tag{2}$$

The power transfer per unit volume, $\dot{q}$, due to thermal conduction, collisional energy exchange, and Ohmic heating, is,

$$\dot{q}_{p,n} = \left(\nabla\cdot\left(k_{\text{therm}}\nabla T_{p,n}\right)\right) \pm \left(\mathbf{R}_{\text{coll},p,n}\cdot\mathbf{u}_{p,n}\right) \pm \left(en_{p,n}\mathbf{u}_{p,n}\cdot\mathbf{E}\right), \tag{3}$$

where the collisional term for each species is,

$$\mathbf{R}_{\text{coll}} = -nm\left(\mathbf{u}_{\text{self}} - \mathbf{u}_{\text{other}}\right)\nu_{\text{coll}}. \tag{4}$$

Because of the assumption that collisions are negligible, we set $k_{\text{therm}} \simeq 0$ and $\mathbf{R}_{\text{coll}} \simeq 0$ to be consistent. Unlike classical ion thrusters and most other plasma thrusters, ion-ion propulsion systems have strong spatial gradients in the density of a given species. Therefore, it may be important to consider the effects of classical gradient-driven mass diffusion (i.e., Fick's law). Therefore, a uniform value of mass diffusivity ($\mathcal{D}$) is included as a parameter to be varied in this simulation.

Because the time-scale of the change of electrodynamic fields (at the speed of light) is much faster than the time-scale of particle motion, we assume the electric field and electric potential are static within each time step. Thus, within a convection-scale time step, the electric potential in the domain is calculated from the values of n_p and n_n at the beginning of that time step inside each cell using the Poisson equation,

$$\nabla^2 V = -\frac{e}{\epsilon_\circ}\left(n_p - n_n\right), \tag{5}$$

and the field is calculated using the electrostatic definition of $\mathbf{E} = -\nabla V$.

This model assumes cylindrical symmetry and, hence, all azimuthal ($\hat{\theta}$) components and all azimuthal derivatives ($\partial/\partial\theta$) are set to zero.

A. Initial and Boundary Conditions

The initial values of densities in the background are set to $n_p = n_n = 5\times10^{12}$ m^{-3}, a value much smaller than the density of the inlet plasma. The initial electric field is set to zero everywhere in the domain. To have a smooth transition into the electrodynamics of the problem, a neutral monatomic iodine gas (I) of $n = 1\times10^{14}$ m^{-3} was injected into the domain. The values after this neutral background has reached equilibrium are set as the initial conditions at $t = 0$ for the simulation. After this, the electrically charged propellant is injected into the domain at $n_p = n_n = 1\times10^{15}$ m^{-3} successively at $f_{\text{bias}} = 1.25$ MHz.

As shown in Fig. 1, the simulation domain begins downstream of the thruster grids. The boundary conditions used in this simulation are as follows:

- $(r = 0, z)$. The radial velocities and the radial electric field are set to zero.
- $(r = R, z)$. All radial gradients of the flowfield and the electric potential are set to zero.
- $(r, z = 0)$. The boundary conditions are set in the following manner, based on the location in the $0 < r \leq R$ range:
  - For $r \leq r_{\text{thrust}}$: The density, velocity, and pressure are set to the thruster exhaust values; because the downstream grid of the thruster is grounded, the electric potential is set to zero.
  - For $r_{\text{thrust}} < r \leq r_{\text{insul}}$: The axial values of velocity and electric field are set to zero.
  - For $r > r_{\text{insul}}$: The axial gradient of the flowfield and the electric potential are set to zero.
- $(r, z = Z)$. The axial gradient of the flowfield and the electric potential are set to zero.

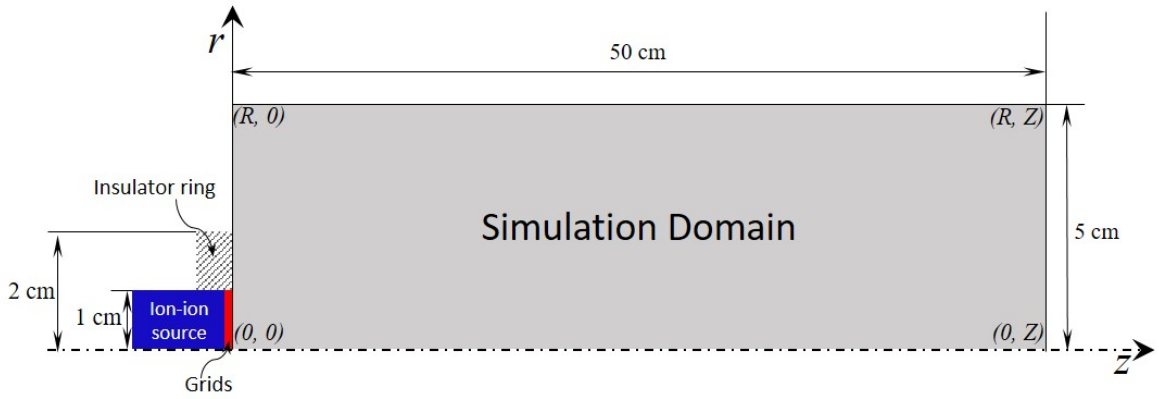

Fig. 1 Schematic of the domain of computation (not to scale).

B. Numerical method

The time variation of Eq. (1) was numerically solved using an explicit time-marching scheme. Because of the strong variations in time caused by alternating injection of positive and negative ions into the domain, it is important to carefully monitor the time accuracy of the simulation. To that end, a 4-step Runge Kutta integration scheme, with a Courant–Friedrichs–Lewy (CFL) value of 0.1 or lower was used in this simulation. The plasma flow was explicitly calculated in time for approximately 100 cycles of the accelerating grid's bias timescale ($T_{\text{bias}} = 1/f_{\text{bias}}$) or until a measurable cyclic steady state was achieved.

The spatial derivatives for the hyperbolic convection problem were calculated using a standard forward difference scheme with numerical dissipation, as described in Ref. [6].

The Poisson equation (Eq. (5)) was solved using a standard Red-Black Successive Over Relaxation (SOR) scheme[7] with a relaxation parameter of $\omega_{\text{opt}} \simeq 1.99$ and a truncation error of $\Delta V_{\text{max}} = 5 \times 10^{-9}$ V. Because the smallest grid dimension was $\Delta r = 5 \times 10^{-4}$ m, this corresponds to a truncation error in the electric field of $\Delta E_{\text{max}} \simeq 10^{-5}$ V/m.

C. GPU Computation

To reduce computation time, GPU-accelerated computing was used in this work. A series of verifications were conducted to validate the computational method used to solve the equations listed above. First, some fundamental linear algebra operations were conducted and benchmarked for speed to verify the accuracy and the efficiency of CPU-GPU communications. Then, the above-mentioned numerical solution techniques to solve elliptic, parabolic, and hyperbolic partial differential equations were tested (in cylindrical coordinates) by solving the Laplace equation, the diffusion equation, and the nonlinear advection equation, respectively. Based on the successes for these test cases, the GPU-accelerated computing platform was utilized to examine the main questions of this research.

IV. Results and Analysis

Resulting contours of number density of ions, $n_{p,n}(r, z)$, their velocity, $\mathbf{u}_{p,n}(r, z)$, their pressure, $p_{p,n}(r, z)$ (which corresponds to the thermal energy, $\mathcal{E}_{\text{therm}}$), and the electric potential, $V(r, z)$ were calculated using the methods discussed in §III.B. To capture the strong time gradients in the flowfield, a CFL value of 0.05 was used to obtain the results shown here. The simulation was deemed to have achieved a cyclic steady state when the results were consistently repeatable for at least 25 cycles ($T_{\text{bias}} = 0.8$ μs). To answer the main questions posed in §I, we simulated four sets of conditions that are summarized in Table 2 and described in the following subsections.

A. Isothermal without mass diffusion

For the purposes of comparison, we first consider the results when the energy conservation equation (the last row in Eq. (1)) is neglected and is replaced with an isothermal assumption that $T_p = T_n = T_{\text{inlet}} = 0.1$ eV (as stated in Table 1). The thermodynamic pressure of the plasma was then calculated using the ideal gas equation. Because some of the earliest publications that examined ion-ion propulsion also invoked an isothermal assumption [8], this functions as a

Table 2 Simulated Cases

Case	Isothermal	Energy Conservation	Mass Diffusion
A	✓		
B	✓		✓
C		✓	
D		✓	✓

baseline that can be useful for comparisons. For the purpose of understanding the effect of diffusion later in §IV.B, we set $\mathcal{D} = 0$ in this baseline case.

Figs. 2, 3, and 4 show that, even under the isothermal assumption, the alternating packets of positive and negative ions interact downstream of the injection. The very strong radial gradient in density outside the plume seen in Figs. 2 & 3 is an artifact of the isothermal assumption, as will be shown later in §IV.C with the inclusion of conservation of energy.

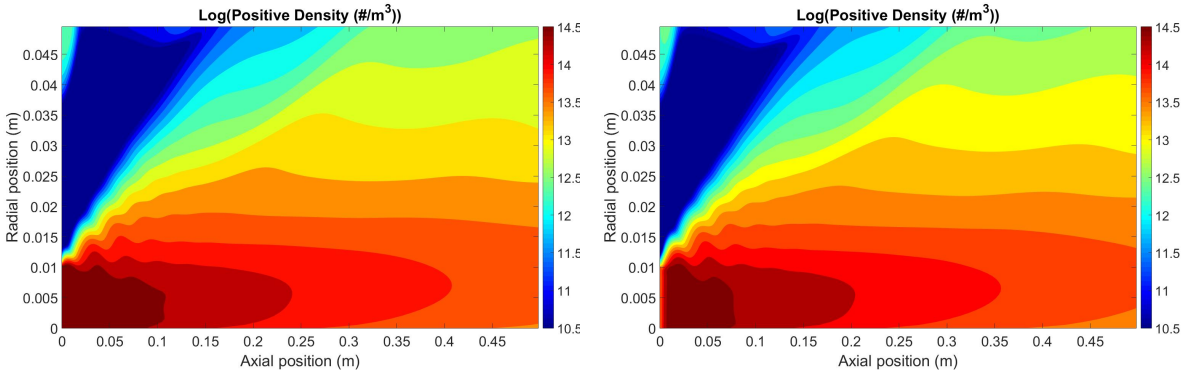

Fig. 2 Case A: Density of positive charges (#/m^3), on a $\log_{10}$ scale, after half and full cycles.

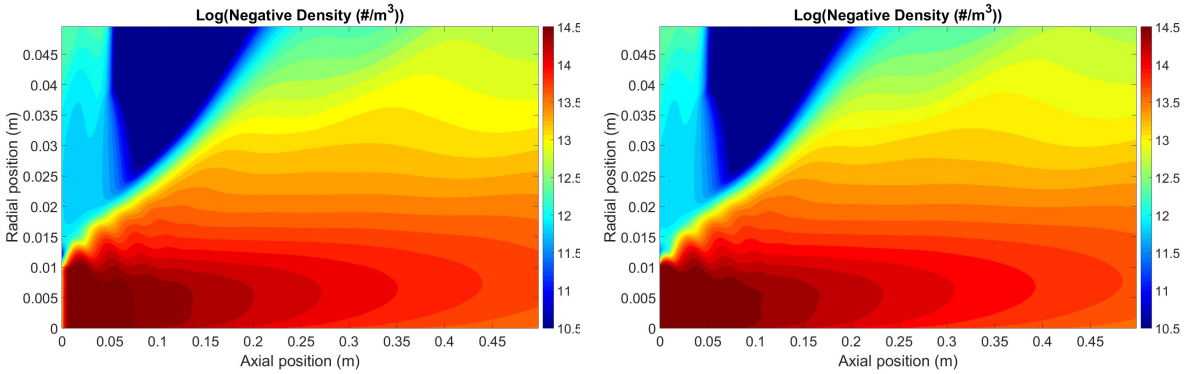

Fig. 3 Case A: Density of negative charges (#/m^3), on a $\log_{10}$ scale, after half and full cycles.

Fig. 4 shows the normalized net charge density ($(n_p - n_n)/n_{\text{inlet}}$) and it is evident that the net charge density decreases quickly after a few packets.

The contour plots of electric potential in the domain after each half-cycle in Fig. 5 show a rapid radial decline in the potential away from the thruster inlet and an oscillatory axial decline over the length of the domain. Furthermore, since the voltage in the domain is always substantially less than the accelerating voltage of 500 V from the thruster grid, the kinetic energy of the ions will be sufficient to pass through the domain by overcoming any electric potential barrier in the domain.

Plots of voltage at the centerline in Fig. 6 show that there are no sharp declines towards $z = 50$ cm to meet the $V = 0$

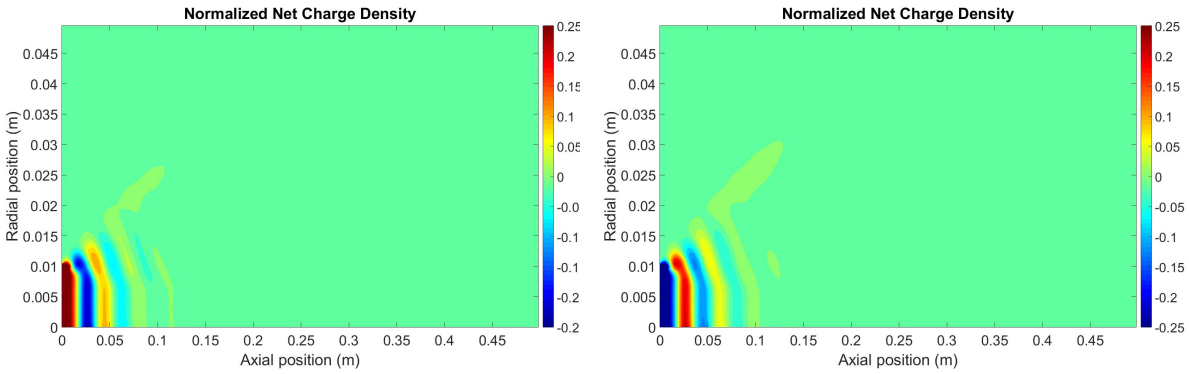

Fig. 4 Case A: Normalized net charge density after half and full cycles.

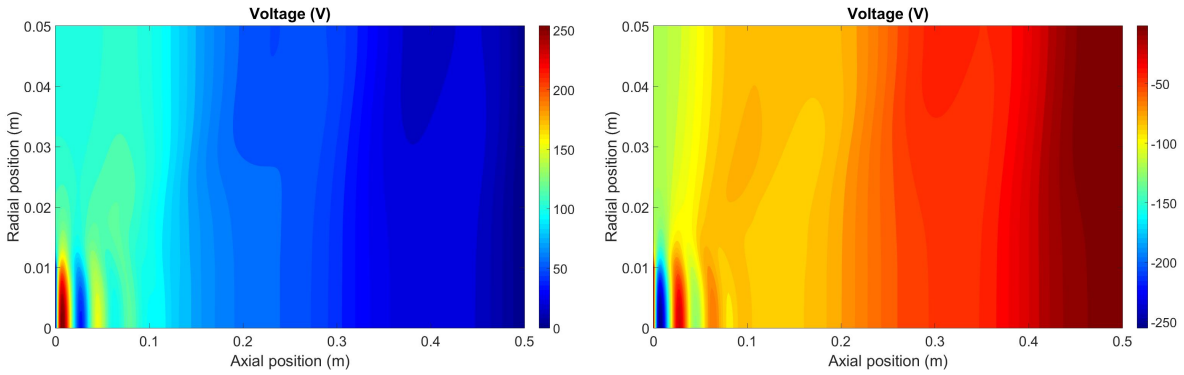

Fig. 5 Case A: Voltage (V) in the domain after half and full cycles.

boundary condition; therefore, the assumption that $V \simeq 0$ at an axial distance of 50× the thruster radius appears to be reasonable. Furthermore, both parts of Fig. 6 (end of half cycle on the left and end of full cycle on the right) resemble a damped wave with a peak value just beyond the inlet. The symmetric peaks measure about ± 250 V at the first packet (at a distance of $z \simeq 1$ cm), ± 150 V at the second packet (at $z \simeq 5$ cm), and ± 120 V at the third packet ($z \simeq 10$ cm), gradually decaying to 0 V over $z = 10$ to 50 cm. In comparison, Oudini, *et al.*[5] observed a ± 120 V peak at the first packet and ± 60 V at the third packet.

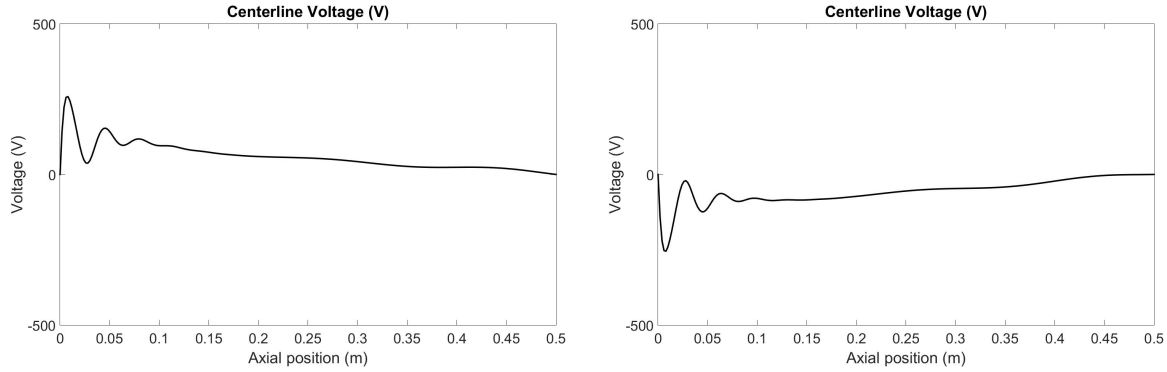

Fig. 6 Case A: Voltage (V) at the centerline after half and full cycles.

Velocity streamlines in Fig. 7 show the trajectories of positive and negative ions in the domain and they clearly indicate a well-defined plasma plume. Examination of the half-cycle (left) and the full-cycle (right) plots of Fig. 7 reveal that the positive and negative ions appear to be on mirror-image trajectories in the region immediately downstream of

the inlet. This behavior is consistent with the presence of strong electric fields in this region. It is also noteworthy that this difference diminishes as the plasma propagates downstream in the domain and the positive and negative charges move in the same direction.

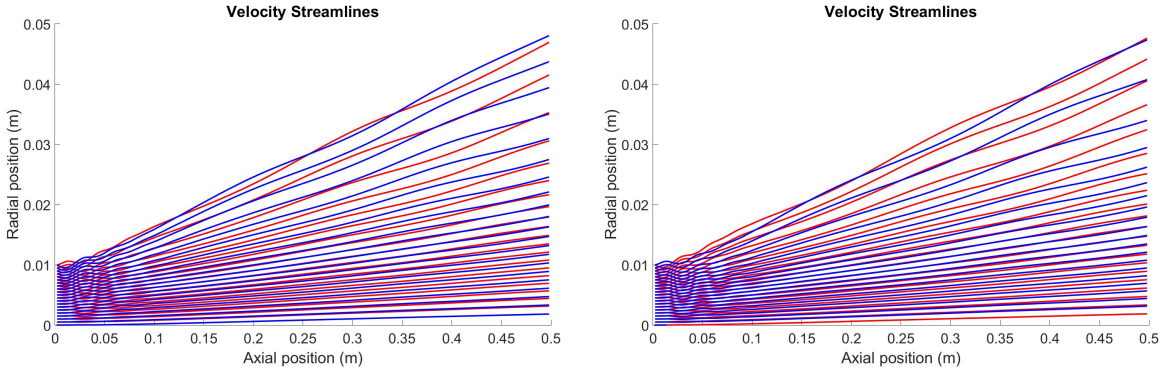

Fig. 7 Case A: Velocity streamlines of positive (red) and negative (blue) charges after half and full cycles.

B. Isothermal with mass diffusion

Starting with the results of §IV.A, we proceed to examine the effects of diffusion. As noted by Oudini, *et al.*[5], collision and transport properties have not been empirically documented well for a plasma comprised of I^+ and I^- ions. To investigate this, we chose a reasonable value of mass diffusivity as a parameter and examined its effects on the results. Here, we present the results when mass diffusivity was set to $\mathcal{D} = 2 \times 10^{-3}$ m^2/s. (For reference, the mass diffusivity of most molecules in air under atmospheric conditions is $O(10^{-5})$ m^2/s.) We specifically examine the effect of mass diffusion on $V \to 0$ away from the inlet.

A comparison of voltages at the centerline in Fig. 8 shows that mass diffusivity has only a minimal influence on voltage at large distances from the inlet ($z \geq 10$ cm) in the isothermal case. A comparison of voltages at the $z = 10$ cm cross section in Fig. 9 shows that mass diffusion changes the electric potential by only $\simeq \pm 5 - 10$ V. Its effect is unremarkable near the inlet ($z < 10$ cm).

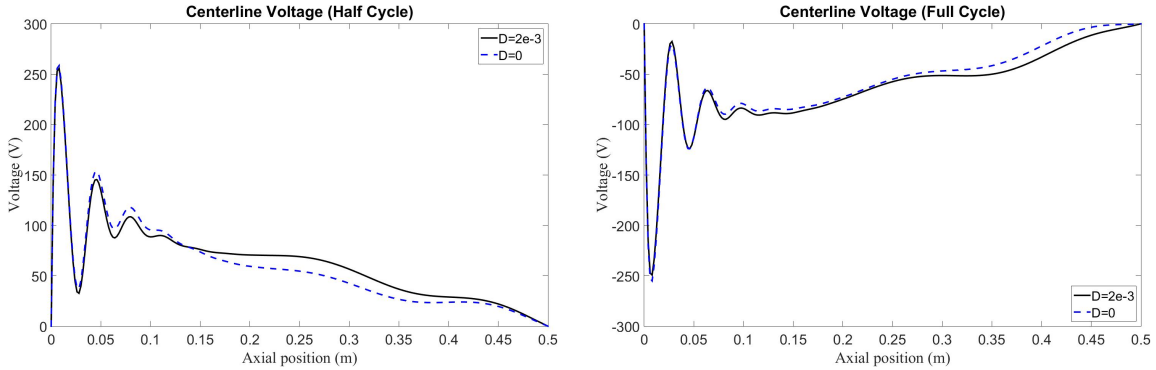

Fig. 8 Case B: Voltage (V) at the centerline after half and full cycles, with and without mass diffusion.

The minimal effect of diffusion on the distribution of ions, and therefore on the voltage, is to be expected. Physically, mass diffusion occurs approximately at the thermal speed and convection occurs approximately at the flow speed. Here, the thermal speed corresponds to a constant temperature of 0.1 eV and the flow speed is of the order of the injection energy of 500 eV. Since the rate of mass diffusion is slower than that of convection by $O(10^3)$, it has only a small effect on the flowfield and the commensurate voltage.

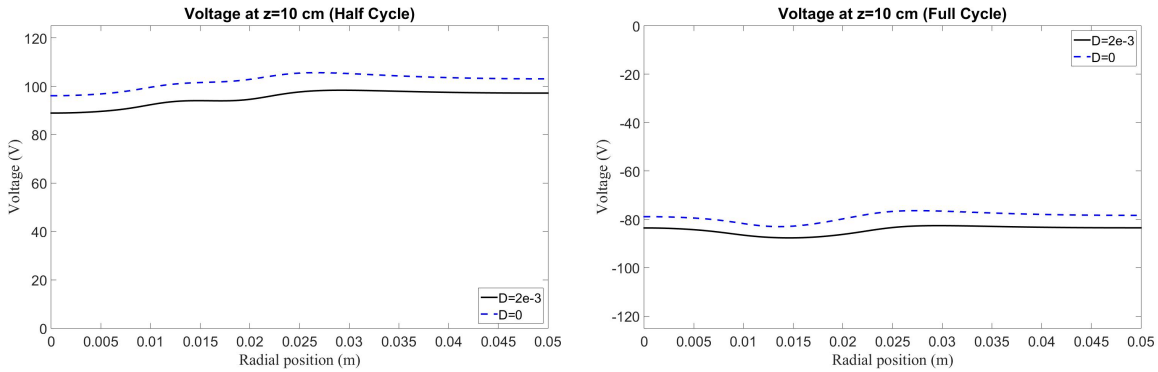

Fig. 9 Case B: Voltage (V) at $z = 10$ cm after half and full cycles, with and without mass diffusion.

C. With energy conservation but without mass diffusion

We will now abandon the isothermal assumption of §IV.A-B and proceed to examine how the flowfield changes with the incorporation of conservation of energy (the last row in Eq. (1)). Under this formulation, the thermodynamic pressure of the plasma is obtained from the energy per volume (Eq. (2)) to be,

$$p = (\gamma - 1)\,(\mathcal{E} - \mathcal{E}_{\text{kin}})\,. \tag{6}$$

A comparison of densities of positive charges (Figs. 2 and 10) and negative charges (Figs. 3 and 11) reveal notable qualitative and quantitative differences between the isothermal and non-isothermal cases. Specifically, abandoning the contrived assumption of a constant temperature and allowing the expanding plume to cool affects the behavior of the flow significantly. While there still exists a clearly defined plume, the sharp radial gradient outside the plume that was seen in Figs. 2 and 3 is muted in Figs. 10 and 11. In other words, the plume divergence has increased in this case. Consequently, due to mass conservation, the axial gradient in density is greater in this case than in the isothermal case.

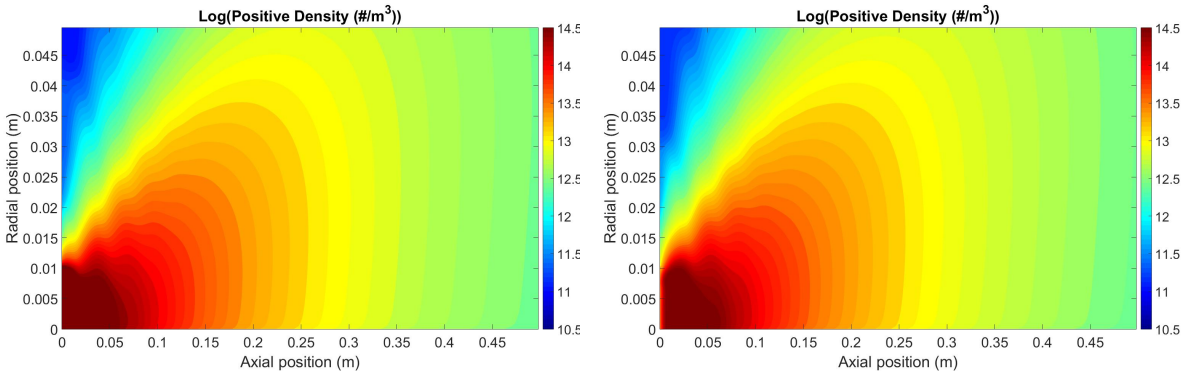

Fig. 10 Case C: Density of positive charges (#/m^3), on a $\log_{10}$ scale, after half and full cycles.

Pressure (Figs. 13 and 14) drops much faster than density (Figs. 10 and 11) in the axial and radial directions, implying an expected decrease in temperature as the plume expands.

A comparison of velocity streamlines in Fig. 15 with the streamlines in the isothermal case (Fig. 7) shows that the cooling of the expanding plume changes the plume significantly. As noted in the discussion earlier on Figs. 10 and 11, the plume divergence is greater here than in the isothermal case.

As noted earlier in the discussion on Figs. 10 and 11, the axial gradient in density is greater in this case than in the isothermal case. Consequently, as a result of Gauss's law and the Poisson equation (Eq. (5)), Figs. 16 and 17 show that the electric potential drops off faster in the axial direction in this case than in the isothermal case (Figs. 5 and 6). Conversely, the centerline values of the voltage at the centerline (Fig. 17) also show a faster decay compared to the isothermal case (Fig. 6). As before, the centerline voltage resembles a damped wave with a peak of about ± 250 V at the first packet, but this peak occurs at $z \simeq 0.6$ cm (compared to $\simeq 1$ cm in the earlier case). The second packet peaks at

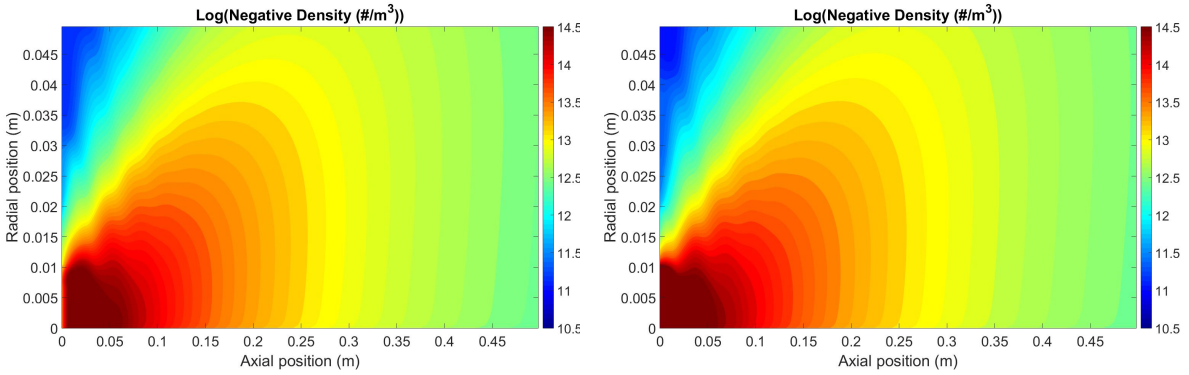

Fig. 11 Case C: Density of negative charges (#/m^3), on a $\log_{10}$ scale, after half and full cycles.

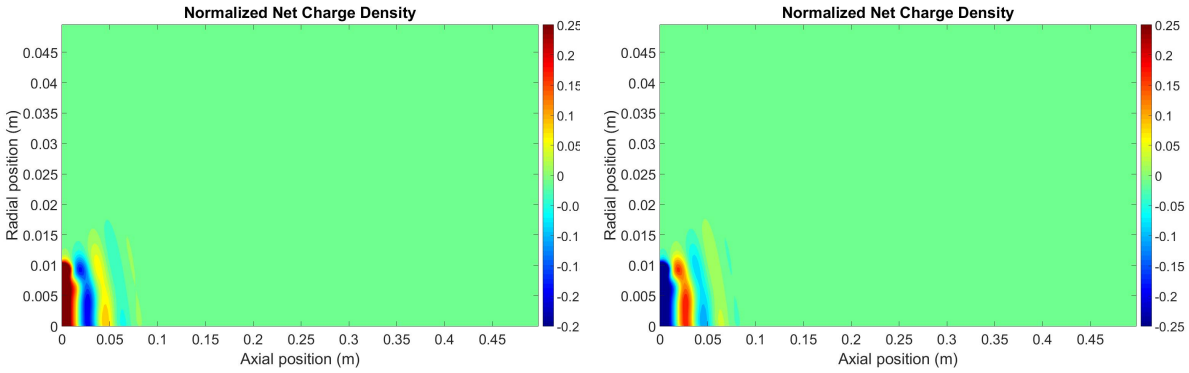

Fig. 12 Case C: Normalized net charge density after half and full cycles.

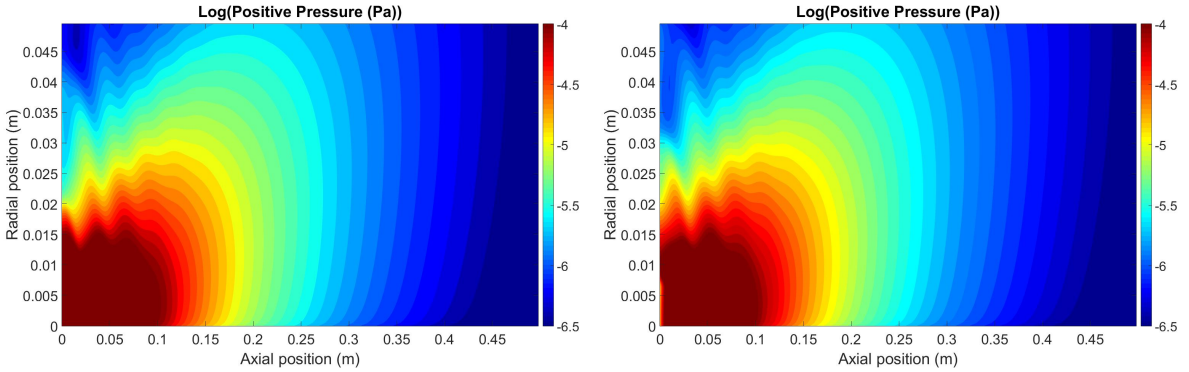

Fig. 13 Case C: Pressure of positive charges (N/m^2), on a $\log_{10}$ scale, after half and full cycles.

$\pm$ 125 V (compared to $\pm$ 150 V for the isothermal case), and it occurs at $z \simeq 4.5$ cm (compared to slightly after $z = 5$ cm in the earlier case). The third packet peaks at $\pm$ 90-95 V (compared to $\pm$ 120 V for the isothermal case), and it occurs at $z \simeq 8.0$ cm (compared to $z \simeq 10$ cm in the earlier case). Again, this can be attributed to the cooling of the plasma in the revised model.

D. With energy conservation and mass diffusion

Under the isothermal assumptions discussed in §IV.A-B, there was a modest impact of mass diffusion at $z \geq 10$ cm. Figs. 18 and 19 show the effects of mass diffusion when the conservation of energy is included. Again, a uniform mass diffusivity of $\mathcal{D} = 2 \times 10^{-3}$ m^2/s was used in the calculations and its effect is examined on the electric potential at the

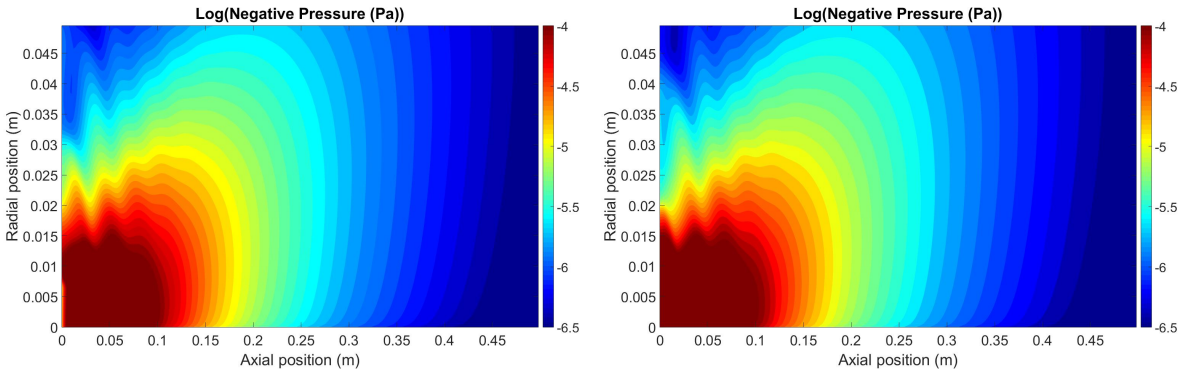

Fig. 14 Case C: Pressure of negative charges (N/m^2), on a $\log_{10}$ scale, after half and full cycles.

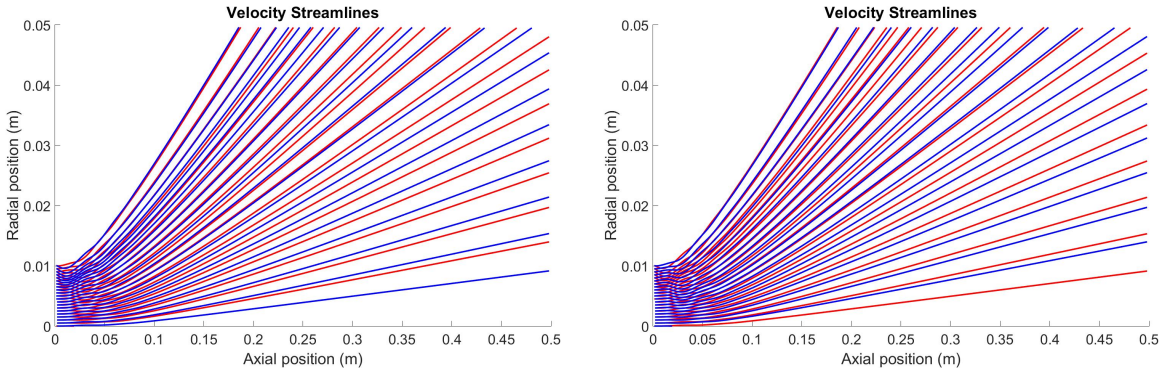

Fig. 15 Case C: Velocity streamlines of positive (red) and negative (blue) charges after half and full cycles.

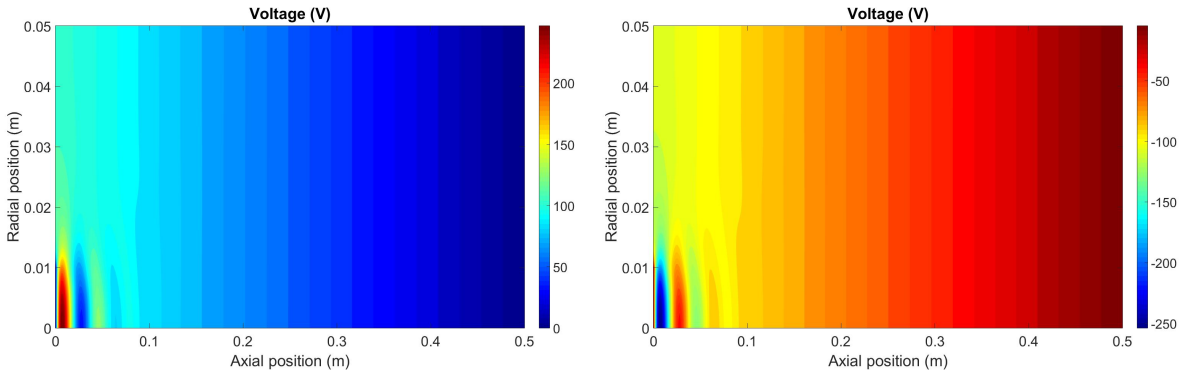

Fig. 16 Case C: Voltage (V) in the domain after half and full cycles.

$r = 0$ and $z = 10$ cm cross sections.

It is clear from these simulations that the effect is only ± 1 V. This is noticeably less than the already small ±5 to 10 V effect of diffusivity in the isothermal case. As noted earlier, mass diffusion occurs approximately at the thermal speed and convection occurs approximately at the flow speed. As the temperature is allowed to cool, the effect of diffusion is further diminished to the point of being negligible.

V. Concluding Remarks

We developed a new two-fluid time-dependent plasma dynamics code using GPU-based computation, which can be utilized to simulate various plasma applications. Using that tool, we simulated the near-field plume of an ion-ion

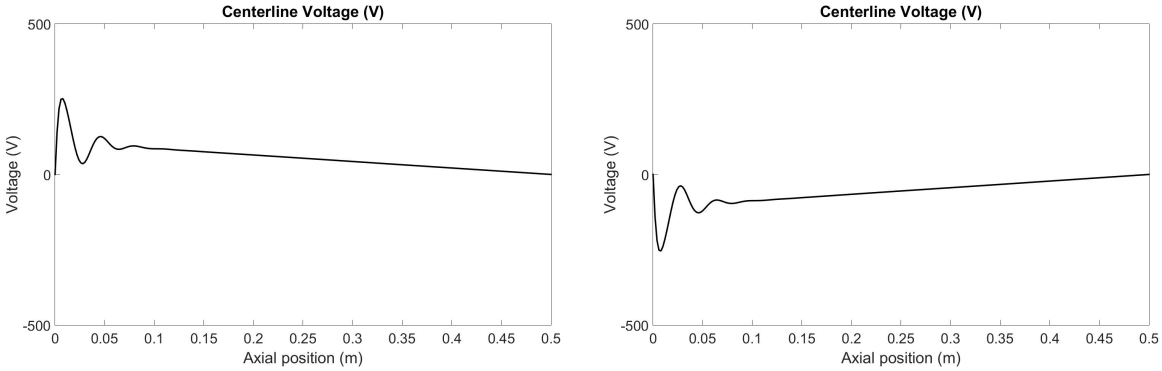

Fig. 17 Case C: Voltage (V) at the centerline after half and full cycles.

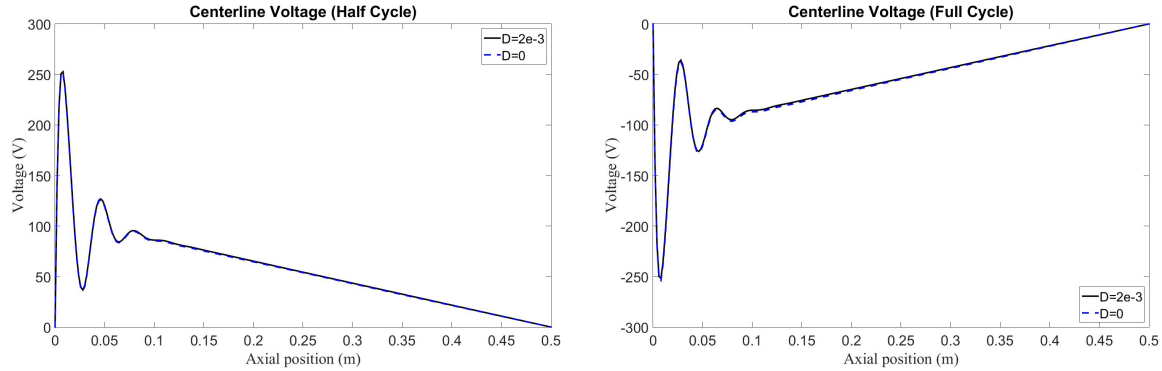

Fig. 18 Case D: Voltage (V) at the centerline after half and full cycles.

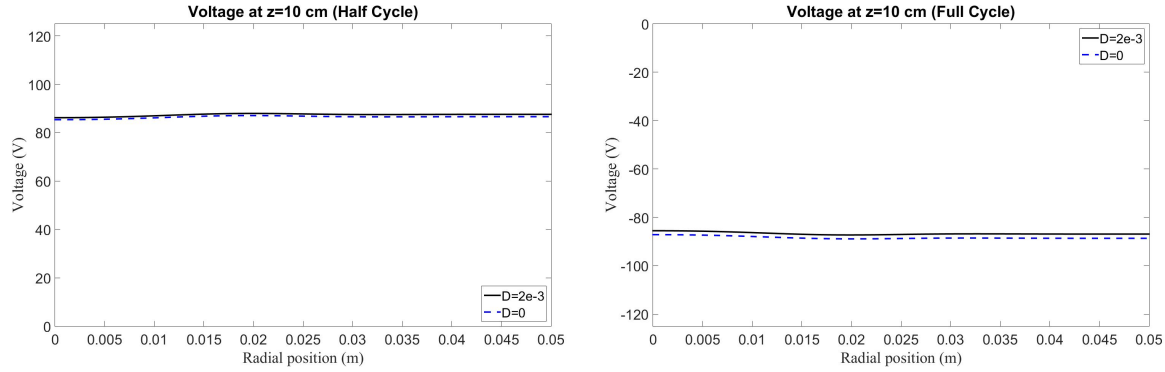

Fig. 19 Case D: Voltage (V) at the centerline after half and full cycles.

propulsion system like that described in Ref. [5]. Our results agree with claim of Ref. [5] that the system achieves a cyclic steady state. Though the time needed to achieve this state varied with the initial condition for the simulation, a cyclic steady state was achieved within ≈ 10 cycles after the initial conditions are convected out of the domain.

We began this inquiry to answer three specific questions (stated at the end of §I), and our results provide some clarity on each.

To answer the question of the electric potential decay downstream of the thruster, our results indicate that it is reasonable to expect the voltage to decay to zero over 50 cm downstream. There are no sharp kinks to meet the $V = 0$ boundary condition. At the third peak (at $z \simeq 8.0$ cm), $V \simeq \pm 90$ V, and it gradually decays to 0 from that point onwards as the distinct packets of positive and negative charges merge.

This leads to the second question of the difference between a 2D-PIC simulation and a two-fluid simulation. The

results of our two-fluid simulation agree with several results of the 2D-PIC simulation of Ref. [5]; notably:

- It is possible to alternatively accelerate oppositely charged ions without the need for an electron-emitting neutralizer,
- A thruster grid bias frequency in the range prescribed by Ref. [5] accelerates a plasma into the domain. This plasma does not face an electric potential hill that would cause stagnation, and
- Voltage decays downstream in an approximately damped-wave fashion with the first peak at $z \simeq 0.6$ cm downstream, the second peak at $z \simeq 4.5$ cm, and the third peak at $z \simeq 8.0$ cm.

There is, however, a noticeable difference between the results of the two models in the voltage decay in the domain. The peak voltages in our two-fluid model are larger than the values from the 2D-PIC models and, therefore, our two-fluid model predicts a longer distance for the neutralization process (and, therefore, voltage decay) than the 2D-PIC model used in Ref. [5]. While our two-fluid model predicts the voltage to be in the ± 90-95 V at the third peak, Ref. [5] finds it to be about ±60 V. Furthermore, our simulations find the voltage at 10 cm downstream to be about $\pm 85 - 90$ V range, while Ref. [5] finds it to be about ± 5-10 V.

That leads to the third question of examining the effect of classical transport mechanisms. Specifically, we examined the effect of mass diffusion. Though the alternating injection of positives and negative ions creates strong spatial gradients in the density of each species at the inlet, it was found that mass diffusion had a negligible effect on the overall flowfield. Thus, classical transport cannot account for the discrepancy in the spatial scale of neutralization (and voltage decay) between our two-fluid simulation and the 2D-PIC simulation of Ref. [5]. Oudini, *et al.*[5] attribute the rapid damping observed in their simulations to Landau damping and its inverse mechanism. This is an explicitly kinetic effect that is not captured in our fluid simulations.

To address the gap between the results of our two-fluid simulation and the 2D-PIC simulation of Ref. [5], we intend to incorporate some kinetic effects into our transport coefficient models. Work by Hammett, *et al.*[9, 10] offer a potential path in bridging the gap between a fluid model and a PIC model. It is worth examining if the effect of Landau damping can be incorporated into a two-fluid model in the form of modified transport coefficients, which would obviate the need to perform more computationally intensive PIC simulations on these types of accelerators.

Acknowledgments

This work was supported by the NASA Washington Space Grant. Computational hardware to support this research was donated by the NVIDIA Corporation.

References

[1] Aanesland, A., Meige, A., and Chabert, P., "Electric propulsion using ion-ion plasmas," *Journal of Physics: Conference Series*, Vol. 162, 2009, p. 012009. doi:10.1088/1742-6596/162/1/012009.

[2] Aanesland, A., Rafalskyi, D., Bredin, J., Grondein, P., Oudini, N., Chabert, P., Garrigues, L., and Hagelaar, G., "The PEGASES gridded ion-ion thruster performance and predictions," *33rd International Electric Propulsion Conference*, ERPS, Washington, DC, 2013.

[3] Gerst, D., Renaud, D., Mazouffre, S., Chabert, P., and Aanesland, A., "E× B probe investigation of the PEGASES thruster ion beam in Xe and SF_6," *33rd International Electric Propulsion Conference*, ERPS, Washington, DC, 2013.

[4] Rafalskyi, D., Popelier, L., and Aanesland, A., "Experimental validation of the dual positive and negative ion beam acceleration in the plasma propulsion with electronegative gases thruster," *Journal of Applied Physics*, Vol. 115, 2014, p. 053301. doi:10.1063/1.4863876.

[5] Oudini, N., Aanesland, A., Chabert, P., Lounes-Mahloul, S., and Bendib, A., "Near-field plume properties of an ion beam formed by alternating extraction and acceleration of oppositely charged ions," *Plasma Sources Sci. Technol.*, Vol. 25, 2016, p. 055013. doi:10.1088/0963-0252/25/5/055013.

[6] Sankaran, K., Martinelli, L., Jardin, S., and Choueiri, E., "A Flux-Limited Numerical Method for the MHD Equations to Simulate Propulsive Plasma Flows," *International Journal of Numerical Methods in Engineering*, Vol. 53, No. 5, 2002, p. 1415. doi:10.1002/nme.343.

[7] Press, W. H., *Numerical Recipes in C*, 3rd ed., Cambridge University Press, 2007, pp. 863–882.

[8] Midha, V., and Economou, D., "Dynamics of ion-ion plasmas under radio frequency bias," *Journal of Applied Physics*, Vol. 90, No. 3, 2001, pp. 1102–1114.

[9] Hammett, G. W., and Perkins, F. W., "Fluid Moment Models for Landau Damping with Applications to the Ion-Temperature-Gradient Instability," *Physical Review Letters*, Vol. 64, No. 25, 1990, pp. 3019–3022.

[10] Hammett, G. W., Dorland, W., and Perkins, F. W., "Fluid models of phase mixing, Landau damping, and nonlinear gyrokinetic dynamics," *Physics of Fluids B*, Vol. 4, No. 7, 1992, pp. 2052–2061.